Polarization-dependent measurement of the near-field distribution of a waveguide with subwavelength aperture

G. Ctistis,[a] O. Schimek, P. Fumagalli, and J. J. Paggel[b]
Institut für Experimentalphysik, Freie Universität Berlin, 14195 Berlin, Germany

(Received 1 June 2005; accepted 28 November 2005; published online 13 January 2006)

The understanding of the near field is essential for scanning near-field optical microscopy. We present here a simple model experiment to examine the polarization of the near field in the proximity of a subwavelength aperture. We make use of microwaves, a fast diode, and different apertures. This allows us to model a polarization-sensitive scanning near-field optical microscope by mapping the field intensity around the aperture in the near-field region. © *2006 American Institute of Physics*. [DOI: 10.1063/1.2160717]

I. INTRODUCTION

Since its invention in the mid 1980s,[1] scanning near-field optical microscopy (SNOM) has become an important experimental tool. By overcoming the diffraction limit, it enables one to resolve objects in the nanometer regime optically. As the idea of the microscope is based on the wave nature of light, the principle of the microscope is not limited to a specific wavelength. As a consequence, near-field microscopes using microwaves have been designed in the past.[2–6] The experimental application of SNOM covers nowadays biological *in vivo* measurements,[7–10] spectroscopic photoluminescence measurements,[11–14] magnetic as well as electric domain imaging,[15–18] and imaging via nonlinear effects.[19–25] Different geometries have been invented during the years.[26,27] The lateral resolution of the technique reaches ~30 nm and is mainly dependent on the aperture size. Despite the wide spread application, only few experiments[28–34] have been performed to understand the optical near field in the proximity of small apertures, which is essential for this technique. The first investigations[28–30] were made for circular apertures in a semiinfinite screen in the microwave region. Subsequent experiments focused either on the intensity of the optical near field,[32,34] the scattering by a subwavelength particle (indirect measurement of the near-field distribution),[31] or on the polarization behavior in the far field.[33] But until now, no experiment has been performed investigating the polarization distribution in the near field directly.

Theory, on the other hand, has been interested in the optical near field (ONF) since the beginning of the 20th century where evanescent fields were predicted.[35] ONF became important in the diffraction theory of small particles or apertures. Therefore a number of calculations are available.[36–40] After invention of the SNOM, theoreticians focused their efforts on understanding the behavior and role of the ONF in image formation and tried to simulate the near field behind or at the surface of a SNOM tip by a numerical solution of Maxwell's equations.[41–48]

In this work, we will present our investigations of the near-field distribution and the polarization in the near field behind a subwavelength aperture in the microwave range. In contrast with optical and x-ray microscopes, no gain in resolution is targeted by using microwaves, but the use of microwaves allows us to work on a macroscopic length scale. Applying a simple detection method we can map the near field behind a subwavelength aperture with a precision of $\lambda/100$ or better while at the same time being able to detect the polarization state of the electromagnetic wave.

The outline of this paper is as follows: A brief discussion of the experimental setup is followed by the discussion of the experimental results. We will mainly present data for the behavior of the polarization in the near-field region behind the aperture. The conclusions will be summarized together with a short outlook on future research.

II. EXPERIMENT

Our experiments were performed using microwaves with a wavelength of $\lambda = 33$ mm generated by a klystron (Spindler and Hoyer), as it is commonly used in physics lectures. A scheme of the setup is shown in Fig. 1(a). The amplitude of the microwave was modulated with a frequency generator (HAMEG HM8030-S) at a frequency of 1362 Hz. The field intensity was detected by a fast diode (Agilent, HSMS-8101) having a size of 1.4×3 mm^2 and was analyzed with a lock-in amplifier (Ithaco-Dynatrac 391A). The diode was glued with resin into a plastic tube and then mounted onto a *xyz* stage allowing positioning in the micrometer range in all three directions. By this metal-free mounting, the distortions of the microwaves by the detector setup were negligible. An aluminum tube served as a waveguide. Aluminum is a perfect mirror in the microwave regime with negligible penetration depth. The length of the tube was 1 m and its inner diameter was 11 cm corresponding to approximately 3.5λ. The ratio of the diameter to the wavelength is similar to the ratio of the diameter of a single-mode fiber ($d = 3$ μm) to visible light ($\lambda = 650$ nm). At the end of the tube, we positioned our subwavelength aperture. It was made from an aluminum sheet with a thickness of 1 mm. In its center, different apertures in size and shape were cut. The circular apertures had diameters from $\lambda/2$ to $\lambda/10$, the oval shaped

[a]Author to whom correspondence should be addressed; electronic mail: georgios.ctistis@physik.fu-berlin.de
[b]Also at Siemens VDO Automotive AG, 93055 Regensburg, Germany.

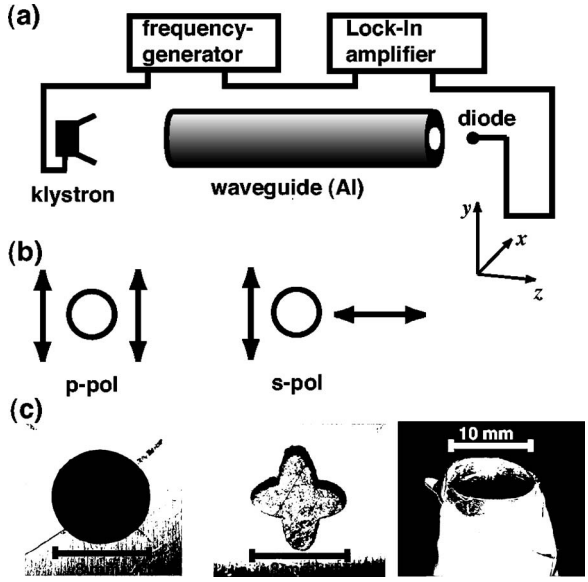

FIG. 1. (a) Schematic drawing of the experimental setup. (b) The pictures indicate the two different measurement geometries. In the parallel configuration (p polarization) the detection direction is parallel to the field polarization. In the perpendicular configuration (s polarization) detection and incident polarization are perpendicular to each other. (c) Pictures of the apertures used. Left: circular aperture with a diameter of 8 mm (=$\lambda/4$), middle: double oval with $\lambda/4$ diameter, and right: tip model with a diameter of 10 mm (=$\lambda/3$).

one $\lambda/4$ at the long side, and $\lambda/8$ at the small one. The model tip, made from aluminum foil, had a circular aperture size of $\lambda/3$ [Fig. 1(c)]. With its apex angle of about 25°, it serves as a model of an aluminum-coated fiber tip. For most aperture sizes, we were able to measure the field intensity starting from inside the waveguide. All measurements were performed within a distance from the aperture of one wavelength. For larger spacing, the intensity of the field was no longer distinguishable from noise. For the polarization-dependent measurements, we rotated the klystron as well as the tube and the aperture by 90°, since the diode could not be rotated after gluing. The polarization geometries are shown in Fig. 1(b).

III. RESULTS AND DISCUSSION

It was first verified that the aluminum tube serves in fact as a waveguide. Since no intensity could be measured outside the waveguide, the coupling efficiency was nearly perfect. The incoming polarization was well maintained inside the tube. However, a small component of an s-polarized field was detectable [Figs. 2(b) and 2(d)]. Further investigations showed that the s-polarized field detected was emitted from the klystron. The field intensities had a ratio E_s/E_p of 1/30. At first glance this might not seem to be a good polarization. But one has to keep in mind that polarization ratios of klystrons are in this region and it is hard to obtain polarization ratios of 10^{-5} as common for quartz optics. By propagating through the tube, the intensity ratio increases to about 1/4. This deviation from initial polarization is mainly due to the reflection of microwaves at the inner surface of the aluminum tube. Upon reflection, a linearly polarized wave becomes elliptically polarized. From the field intensities, we

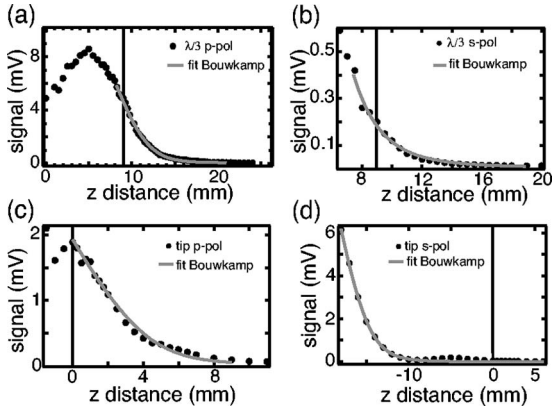

FIG. 2. Plots of the measured field intensity against distance. [(a) and (b)] $\lambda/3$ aperture in p- and s-polarization configurations, respectively. [(c) and (d)] Tip in p- and s-polarization configurations, respectively. The circles are the experimental values while the fits have been done with Bouwkamp's theory. The vertical lines denote the position of the hole.

estimate an ellipticity of about 10°, which is a reasonable value. Figure 2 displays the distance-dependent measurements of the field intensity. Figures 2(a) and 2(b) are for a plane aperture of $\lambda/3$ in size and Figs. 2(c) and 2(d) for the tip. Behind the aperture, the field decreases monotonically. Fitting the data with Bouwkamp's theory of diffraction by small holes[39] yields a very good agreement between theory and experiment, yet not all features inside the aperture can be explained by this theory. This features, i.e., a visible maximum inside the waveguide [Fig. 2(a)] and local maximum and minimum in the tip [Fig. 2(d)], may be explained by standing waves and the extinction of guided modes. This assumption is supported by calculations.[49]

In Fig. 3, we map the intensity around the aperture for two different polarization directions at a distance of 2 mm ($\lambda/16$) from the aperture, which is in the near-field region of the aperture. The intensity distribution for a circular aperture

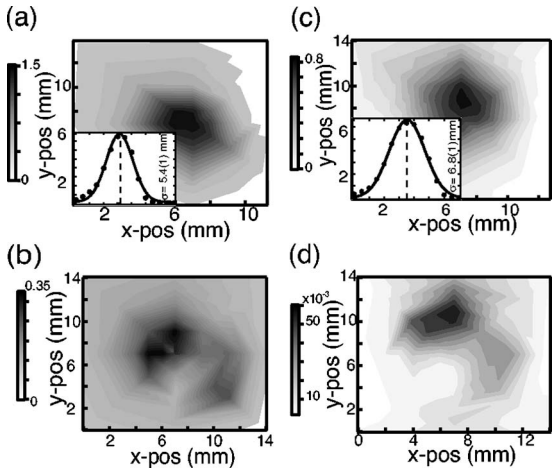

FIG. 3. Polarization-dependent measurements at a distance of 2 mm from the aperture. Intensity maps for a circular aperture (diameter: $\lambda/4$) in (a) p- and (b) s-polarization configurations. The inset in (a) shows a line profile. The width of the curve indicates a resolution better than $\lambda/10$. The s polarization shows an asymmetric field distribution with two maxima. Intensity maps for (c) p and (d) s polarizations for the tip. Inset in (c): line profile indicating a resolution of about $\lambda/10$. In the case of s polarization, the field distribution shows again an asymmetric behavior.

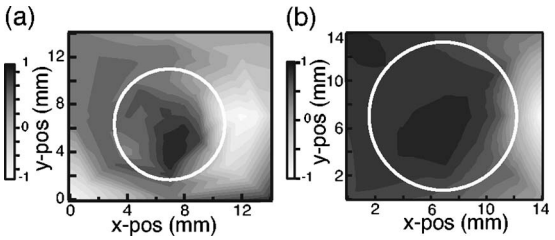

FIG. 4. Two-dimensional plots of the polarization. Positive values indicate *p*-polarized light, while *s* polarization is visualized by negative values. (a) $\lambda/4$ circular aperture. The white circle marks the area of the aperture. The data are taken from Figs. 3(a) and 3(b). Two regions are visible with opposite polarization. (b) Polarization map for the tip. The white circle again marks the area of the aperture. Data have been taken from Figs. 3(c) and 3(d).

with a diameter of $\lambda/4$ in *p* and *s* polarizations is displayed in Figs. 3(a) and 3(b) and the behavior behind the tip in Figs. 3(c) and 3(d). Except for the decrease in intensity, the behavior was similar for other distances, i.e., the shapes of the fields were conserved. The center of the aperture is located at (7, 7.5) for the circular aperture and at (7, 8) for the tip. For both cases it is obvious that the field is fairly undistorted for *p* polarization [Figs. 3(a) and 3(c)]. We have a nearly circular-shaped field, decreasing in intensity with increasing radial distance from the center. The insets are taken along the *x* direction at the center value of the *y* position. Both show a Gaussian profile. The full widths at half maximum of the curves (5.4 mm in the case of the plane aperture and 6.8 mm for the tip) display directly the lateral resolution of the experiment amounting to about $\lambda/10$. The only difference between the planar aperture and the tip is that for the tip the maximum intensity is slightly shifted from the center of the hole. This is probably an effect of the imperfect shape of the tip. A completely different behavior is visible for the *s*-polarized fields [Figs. 3(b) and 3(d)]. Here, we have a highly distorted field for both setups. In the case of the plane aperture [Fig. 3(b)], the field intensity has a maximum at the center of the hole and an additional one at its edge. The maxima are at an angle of 45°. Since the aperture has no visible inhomogeneity and a negligible roughness compared to the wavelength, the second maximum must have its origin in higher-order moments. For the tip [Fig. 3(d)] a comparable behavior is visible. The origin of the higher-order moments is understandable taking into account the origin of the *s*-polarized field. It emerges from reflections yielding a polarization rotation of the incoming wave field. However, this does not explain why one region is favored.

A question arising from the intensity plots is if polarization-dependent measurements, as done in SNOM, are possible. We, therefore, calculated from the plots of the *p* and *s* polarizations the resulting degree of polarization *P* according to

$$P = \frac{I_P - I_S}{I_P + I_S}, \tag{1}$$

where I_P and I_S are the field intensities of the *p*- and *s*-polarized waves, and normalized the result with the total intensity. Figure 4 shows the result of this calculation. Positive values denote *p* polarization while negative values stand

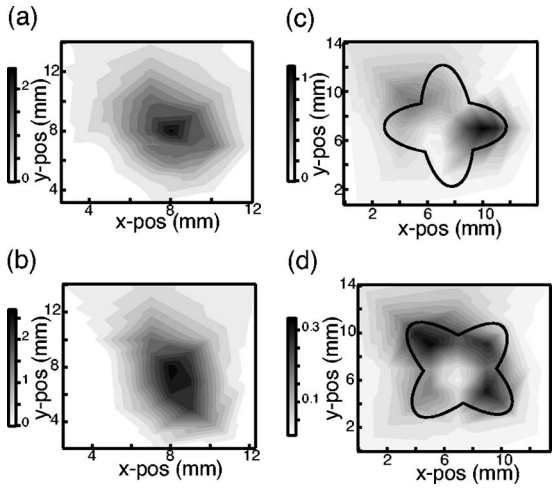

FIG. 5. Intensity maps for different apertures. Upper row: *p* polarization. Lower row: *s* polarization. All measurements took place at a distance of 2 mm from the aperture. [(a) and (c)] double oval; [(b) and (d)] double oval rotated by 45°. The apertures are marked in the plots.

for *s* polarization. The white circles in the plots denote the aperture boundaries. In Fig. 4(a), showing the plane aperture, the polarization is highly inhomogeneous. In the center of the hole we find completely *p*-polarized light while at the edge to the right it is mainly *s* polarized, as it is clear by comparing Figs. 3(a) and 3(b). In SNOM, image formation results from the integral intensity of the illuminated area. Not only contributions from within the aperture play a role but also from its vicinity. Calculating the integral of the whole area in Fig. 4 gives us therefore information on the polarization degree of the measurement. For the plane aperture a polarization degree of roughly 45%, due to the high intensity of the *s*-polarized light, is not very promising for image formation. The situation changes using the tip where a polarization degree of 90% is obtained. This result shows clearly that polarization-dependent measurements are possible with such a setup. To understand, if the aperture's shape plays a significant role in the field detected, we changed the aperture and measured the field distribution behind a double oval [displayed in the center of Fig. 1(c)]. Figures 5(a) and 5(c) show the results for *p* and *s* polarizations, respectively. In the *p*-polarized case, the field distribution around the aperture is again homogeneous and circular shaped. The aperture does not affect the field. If we assume a dipolar field with the polarization axis parallel to one branch of the double oval, it is not surprising to receive this field distribution. In the case of *s* polarization we measure a more complicated field distribution. Now two intensity maxima can be seen lying in the vicinity of the two axes of the aperture but only on one side. In the center of the aperture, we measure nearly no intensity indicating a node in the field distribution. This behavior can be explained if one takes into account not only dipole moments but also higher-order multipoles. Rotating the aperture by 45° results in field distributions displayed in Figs. 5(b) and 5(d). In the *p*-polarized case [Fig. 5(b)], the distribution is now a little distorted but the aperture is not imaged. The *s*-polarized case is more interesting. Now, four maxima exist, all lying at the ends of the double oval. In the center we find an intensity node again. This picture shows the field distri-

bution of a quadrupole and corroborates the assumption of generation of higher-order multipoles. If *p*- and *s*-polarized field distributions are dominated by dipole and quadrupole moments, respectively, one could expect a distance dependence of the degree of polarization in the near field. However, the entire intensity distribution follows an exponential decrease so that the difference in the polynomial order is not distinguishable.

IV. SUMMARY

In summary, we presented data of the investigation of the near field behind a subwavelength aperture. Since at optical dimensions a polarization-dependent intensity mapping of the near field behind the aperture is not possible, we use a simple experiment in the microwave region. We were able to show that the polarization of the field behind an aperture is maintained and, although integrating over an area, SNOM measurements are possible. We have shown, that the *p*-polarized field is nearly not affected by the aperture's size and form but the *s*-polarized field shows a strong dependence. This has been explained with the generation of higher-order multipole moments.

Future experiments shall increase the sensitivity of the measurements to give a more detailed picture of the nature of the two fields. The behavior and role of aperture's size and form will be examined with different apertures. Finally, the design of the aluminum tube will be optimized to be more fiberlike.

[1]D. W. Pohl, W. Denk, and M. Lanz, Appl. Phys. Lett. **44**, 651 (1984).
[2]E. A. Ash and G. Nichols, Nature (London) **237**, 510 (1972).
[3]F. Albiol, S. Navas, and M. V. Andres, Am. J. Phys. **61**, 165 (1993).
[4]T. Wei, X.-D. Xiang, W. G. Wallace-Freedman, and P. G. Schultz, Appl. Phys. Lett. **68**, 3506 (1996).
[5]C. P. Vlahacos, R. C. Black, S. M. Anlage, A. Amar, and F. C. Wellstood, Appl. Phys. Lett. **69**, 3272 (1996).
[6]A. Imtiaz, M. Pollak, S. M. Anlage, J. D. Barry, and J. Melngailis, J. Appl. Phys. **97**, 044302 (2005).
[7]H. Muramatsu, K. Homma, N. Yamamoto, J. Wang, K. Sakata-Sogawa, and N. Shimamoto, Mater. Sci. Eng., C **12**, 29 (2000).
[8]W. H. J. Rensen, N. F. van Hulst, and S. B. Kämmer, Appl. Phys. Lett. **77**, 1557 (2000).
[9]T. Yoshino *et al.*, Ultramicroscopy **97**, 81 (2003).
[10]M. Antagnozzi, M. D. Szczelkun, A. D. L. Humphris, and M. J. Miles, Appl. Phys. Lett. **82**, 2761 (2003).
[11]V. Emiliani, F. Intoni, Ch. Lienau, and T. Elsaesser, Phys. Rev. B **64**, 155316 (2001).
[12]Y. Kanemitsu, T. J. Inagaki, M. Ando, K. Matsuda, T. Saiki, and C. W. White, Appl. Phys. Lett. **81**, 141 (2002).
[13]J. M. Kim, T. Ohtani, and H. Muramatsu, Surf. Sci. **549**, 273 (2004).
[14]J. M. Gerton, L. A. Wade, G. A. Lessard, Z. Ma, and S. R. Quake, Phys. Rev. Lett. **93**, 180801 (2004).
[15]T. J. Silva, S. Schultz, and D. Weller, Appl. Phys. Lett. **65**, 658 (1994).
[16]G. Eggers, A. Rosenberger, N. Held, and P. Fumagalli, Surf. Interface Anal. **25**, 438 (1997).
[17]G. Eggers, A. Rosenberger, N. Held, A. Münnemann, G. Güntherodt, and P. Fumagalli, Ultramicroscopy **71**, 249 (1998).
[18]G. Meyer, T. Crecelius, A. Bauer, I. Mauch, and G. Kaindl, Appl. Phys. Lett. **83**, 1394 (2003).
[19]I. I. Smolyaninov, A. V. Zayats, and Ch. C. Davis, Phys. Rev. B **56**, 9290 (1997).
[20]B. A. Nechay, U. Siegner, M. Achermann, H. Bielefeldt, and U. Keller, Rev. Sci. Instrum. **70**, 2758 (1999).
[21]A. V. Zayats and V. Sandoghdar, Opt. Commun. **178**, 245 (2000).
[22]D. Wegener, U. Conrad, J. Güdde, G. Meyer, T. Crecelius, and A. Bauer, J. Appl. Phys. **88**, 2166 (2000).
[23]I. I. Smolyaninov, H. Y. Liang, C. H. Lee, and C. C. Davis, J. Appl. Phys. **89**, 206 (2001).
[24]V. Emiliani, T. Guenther, C. Lienau, R. Nötzel, and K. H. Ploog, J. Microsc. **202**, 229 (2001).
[25]W. Dickinson, S. Takahashi, D. McHugh, R. Atkinson, R. Pollard, and A. V. Zayats, J. Appl. Phys. **97**, 033505 (2005).
[26]B. Hecht, B. Sick, U. P. Wild, V. Deckert, R. Zenobi, O. J. F. Martin, and D. Pohl, J. Chem. Phys. **112**, 7761 (2000).
[27]Y. Inouye, Top. Appl. Phys. **81**, 29 (2001).
[28]C. L. Andrews, Phys. Rev. **71**, 777 (1947).
[29]C. L. Andrews, J. Appl. Phys. **21**, 761 (1950).
[30]M. J. Ehrlich, S. Silver, and G. Held, J. Appl. Phys. **26**, 336 (1955).
[31]E. Betzig and R. J. Chichester, Science **262**, 1422 (1993).
[32]G. Kolb, K. Karrai, and G. Abstreiter, Appl. Phys. Lett. **65**, 3090 (1994).
[33]C. Obermüller, K. Karrai, G. Kolb, and G. Abstreiter, Ultramicroscopy **61**, 171 (1995).
[34]C. Obermüller and K. Karrai, Appl. Phys. Lett. **67**, 3408 (1995).
[35]A. Sommerfeld, Ann. Phys. (Paris) **44**, 12 (1914).
[36]J. A. Stratton and L. J. Chu, Phys. Rev. **56**, 99 (1939).
[37]H. A. Bethe, Phys. Rev. **66**, 163 (1944).
[38]H. Levine and J. Schwinger, Phys. Rev. **74**, 958 (1948).
[39]C. J. Bouwkamp, Philips Res. Rep. **5**, 321 (1950).
[40]C. J. Bouwkamp, Rep. Prog. Phys. **17**, 35 (1954).
[41]U. Dürig, D. W. Pohl, and F. Rohner, J. Appl. Phys. **59**, 3318 (1986).
[42]C. Girard and A. Dereux, Rep. Prog. Phys. **59**, 657 (1996).
[43]O. J. F. Martin, J. Microsc. **194**, 235 (1999).
[44]C. Girard, C. Joachim, and S. Gauthier, Rep. Prog. Phys. **63**, 893 (2000).
[45]G. Lévêque, G. Colas des Francs, C. Girard, J. C. Weeber, C. Meier, C. Robilliard, R. Mathevet, and J. Weiner, Phys. Rev. E **65**, 036701 (2002).
[46]O. J. F. Martin and M. Paulus, J. Microsc. **205**, 147 (2002).
[47]A. Bouhelier, J. Renger, M. R. Beversluis, and L. Novotny, J. Microsc. **210**, 220 (2003).
[48]L. Vaccaro, L. Aeschimann, U. Staufer, H. P. Herzig, and R. Dändliker, Appl. Phys. Lett. **83**, 584 (2003).
[49]A. Castiaux, A. Dereux, J.-P. Vigneron, C. Girard, and O. J. F. Martin, Ultramicroscopy **60**, 1 (1995).